Blind image deblurring with noise-robust kernel estimation

Chanseok Lee[1], Jeongsol Kim[1], Seungmin Lee[1], Jaehwang Jung[2], Yunje Cho[2], Taejoong Kim[2], Taeyong Jo[2], Myungjun Lee[2], and Mooseok Jang[1,3]

[1] Department of Bio and Brain Engineering, KAIST, Daejeon, South Korea
[2] Advanced Process Development Team 4, Semiconductor R&D Center, Samsung Electronics, South Korea
[3] KAIST Institute for Health Science and Technology, KAIST, Daejeon, South Korea
`{cslee, mooseok}@kaist.ac.kr`

Abstract. Blind deblurring is an ill-posed inverse problem involving the retrieval of a clear image and blur kernel from a single blurry image. The challenge arises considerably when strong noise, where its level remains unknown, is introduced. Existing blind deblurring methods are highly susceptible to noise due to overfitting and disturbances in the solution space. Here, we propose a blind deblurring method based on a noise-robust kernel estimation function and deep image prior (DIP). Specifically, the proposed kernel estimation function effectively estimates the blur kernel even for strongly noisy blurry images given a clear image and optimal condition. Therefore, DIP is adopted for the generation of a clear image to leverage its natural image prior. Additionally, the multiple kernel estimation scheme is designed to address a wide range of unknown noise levels. Extensive experimental studies, including simulated images and real-world examples, demonstrate the superior deblurring performance of the proposed method. The official code is uploaded in `https://github.com/csleemooo/BD_noise_robust_kernel_estimation`.

Keywords: Blind deblurring · Deep image prior · Gaussian noise

1 Introduction

Optical imaging systems such as brightfield microscopes, fluorescence microscopes, or scanning electron microscopes (SEM) have a crucial role in histopathology, inspection, and clinical or biological research by providing complicated structural information of target imaging samples with high-resolution images. However, perturbation or misalignment (e.g. defocus or aberrations) of the imaging system due to its instability or systemic error brings blurry effects on the captured image. Furthermore, additive Gaussian Noise severely degrades the captured image quality. Such degradation process can be described as follows:

$$y_m = x * h + n_g \tag{1}$$

, where $y_m \in \mathbb{R}^N$ is measured blurry and noisy image, $x \in \mathbb{R}^N$ is a clear image, $*$ denotes the convolution operator, $h \in \mathbb{R}^M$ is blur kernel or point spread function (PSF) of the imaging system, and n_g is additive noise. Retrieving clean and focused image x as well as blur kernel h from a single degraded image y_m is well known as *blind deconvolution* or *blind image deblurring* and has been actively investigated for decades due to its ill-posedness. Although many previous approaches such as edge-selection-based method [5,16,37,38] or MAP-based approach [4,15,18,23,29–31,41,44] show promising results, deblurring performances significantly drop as the noise level increases.

In general, there is a trade-off when simultaneously trying to eliminate both the blur effect and noise. For example, when focusing on removing the blur effect, the estimated image may be severely corrupted by noise or other high-frequency artifacts. On the other hand, when focusing on noise removal, there is a tendency to overly emphasize smoothness, compromising the fine details of the image. So, balancing the strength of deblurring and noise suppression is important to successfully reconstruct x and h. Moreover, in cases where the noise level cannot be accurately determined, the difficulty of the deblurring task increases significantly.

This paper aims to address the challenge of blind deblurring in the presence of strong and an unknown noise level. Instead of relying on sharp edge-selective maps or prior information to estimate the blur kernel, we introduce a novel kernel estimation function. This function analytically computes the blur kernel when provided with a clear image, blurry image, and noise suppression factor. The first characteristic of the proposed function is its ability to estimate the blur kernel effectively even in scenarios with strong noise. Specifically, the noise suppression factor included in the kernel estimation function is pivotal in mitigating noise, and its optimal condition is derived accordingly. To further ameliorate this characteristic, we designed a multiple kernel estimation scheme, which effectively handles a wide range of noise levels, to perform blind deblurring even in situations where the noise level is unknown. The second characteristic is that the estimation of only the clear image is sufficient for estimating a blur kernel. In other words, the amount of information required for solving a blind deblurring problem is much less than that needed by conventional methods, and we validated this through maximum a posteriori (MAP) analysis. This characteristic is fully leveraged by employing DIP, known as one of the most effective methods for capturing priors of natural images and solving inverse mapping problems [39]. The inherent robustness of DIP to noise, combined with the noise-robust multiple kernel estimation scheme, enables superior performance in blind deblurring tasks.

The main contributions of this paper can be summarized as follows:

1. We propose a noise-robust kernel estimation function along with its optimal conditions, enabling the analytical acquisition of an ideal blur kernel when provided with a clear image and a blurry image.
2. We design a multiple kernel estimation scheme to address a wide range of unknown noise levels.

3. We adopt DIP to leverage the natural image prior captured by the hand-crafted neural network for the generation of both a clear image and intermediate images which are used for estimating blur kernels.
4. The experimental results and detailed analysis with simulation and experimental data consistently demonstrate that the proposed method outperforms in blind deblurring tasks, particularly in scenarios where strong noise exists.

2 Related works

MAP-based method The Blind deblurring problem has been actively investigated for decades as a blurred image can be explained as many pairs of clear images and blur kernels. One of the prevalent approaches involves addressing the problem within the MAP framework consisting of priors of clear image and blur kernel. For example, Krishnan *et al.* [18] proposed the normalized sparsity regularization l_1/l_2 to maximize the prior of clear image. Pan *et al.* [30] adopted the dark channel on the premise that the dark channel of a clean image exhibits much sparsity compared to the blurred image. Other sparsity constraints such as TV-regularization [31], l_0 norm [29], l_p norm [15, 44] have been proposed to regularize the solution space of a clear image. Also, there have been some prior works to regularize the blur kernel estimation such as sparsity priors [23, 44]. Also, equality constraint $\sum h = 1$ and non-negativity $h \geq 0$ are imposed to blur kernel estimation for the stability of convergence.

Recently, DIP has been incorporated into the MAP framework for blind deblurring problems. Specifically, the inherent capacity of a well-designed neural network to capture image statistics is leveraged by substituting the regularization function with the neural network itself. For example, Ren *et al.* [33] adopts double-DIP [11] to infer the latent information of clear image and blur kernel. The elaborately designed generators have shown state-of-the-art blind deblurring performance without requiring explicit knowledge of clear image and blur kernel. Bredell *et al.* [3] incorporates the Wiener filter as a guide during the training of the DIP, effectively improving deblurring performance.

Noise-blind deblurring The deblurring problem becomes more challenging when the noise level is not accurately known. One expected approach is to estimate the noise level first and then apply state-of-the-art deblurring methods. However, the estimation of the noise level in blurry images has not yet been reported, making it difficult to apply. To remedy this problem, methods such as adopting Bayesian estimator [1,14], variational expected maximization-based method [28], and other few training-based methods [9,19,35] have been proposed and shown state-of-the-art deblurring performances.

3 Method

3.1 Wiener deconvolution method

The core idea of the Wiener deconvolution method is to find an inverse filter $w_{h\to x}$ that can estimate true signal $\hat{x}$. The optimal inverse filter can be derived from error minimization of the difference between the inverse filtered image $\hat{x}$ and target image x: $\epsilon = \mathbb{E}[|X - \hat{X}|^2]$, where $\mathbb{E}$ denotes expectation, X and $\hat{X}$ is Fourier transform of x and $\hat{x}$, respectively. The estimated true signal can be acquired from the following equation:

$$\hat{X} = \frac{\bar{H}}{|H|^2 + \eta} Y_m \tag{2}$$

, where $\bar{\cdot}$ denotes complex conjugation and η is the ratio between the mean power spectral density (mPSD) of noise and signal. As Eq. (2) is simple but effective in reducing noise and deblur the degraded image, many of previous works [3, 10, 24, 42] employed Wiener filter to their deblurring framework. Inspired by this, we derive the following kernel estimation function.

3.2 Noise-robust kernel estimation function

Claim 1. *Given blurry image y_m and clean image x, the blur kernel $\widehat{h}$ can be estimated by $\widehat{H} = \frac{\overline{X}}{|X|^2+k} Y_m$, where $\widehat{H}$, Y_m, and X are Fourier transform of $\widehat{h}$, y_m, and x, respectively, and k is the ratio between the mean power spectral density of noise and blur kernel.*

Proof. We formulated the following mean squared error to derive a kernel estimation function using an inverse filter $w_{x\to h}$.

$$\epsilon = \mathbb{E}[|H - \widehat{H}|^2] = \mathbb{E}[|H - \widehat{W}[HX + N_g]|^2] = \mathbb{E}[|[1 - \widehat{W}X]H - \widehat{W}N_g|^2] \tag{3}$$

Here, the subscript of an inverse filter w is dropped for the sake of simplicity. As we assume that the noise n has zero mean and independent to blur kernel k, Eq. (3) can be simplified as

$$\epsilon = (1 - \widehat{W}X)\overline{(1 - \widehat{W}X)} S_H + \widehat{W}\overline{\widehat{W}} S_{N_g} \tag{4}$$

, where $S_H = \mathbb{E}[|H|^2]$ and $S_{N_g} = \mathbb{E}[|N_g|^2]$ are the mPSD of blur kernel and noise, respectively, and $\bar{\cdot}$ denotes complex conjugation. Eq. (4) can be solved by computing the derivative of ϵ with respect to $\widehat{W}$ to become zero. Now, we can calculate the $\widehat{H}$ from X and Y_m as follows:

$$\widehat{H} = \widehat{W} Y_m = \frac{\overline{X}}{|X|^2 + k} Y_m \tag{5}$$

, where noise suppression factor k is the ratio between the mPSD of noise and blur kernel. The final $\hat{h}$ can be acquired by applying an inverse Fourier transform

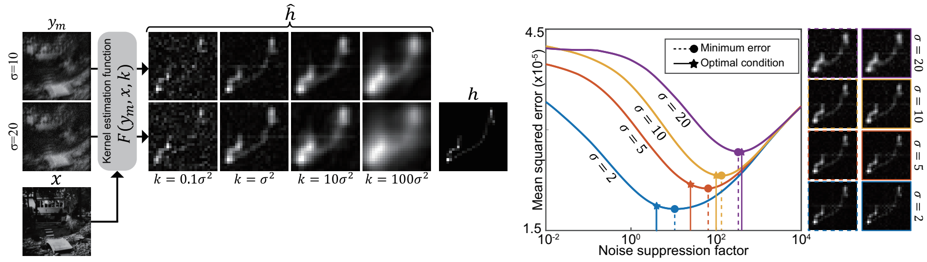

(a) (b)

Fig. 1: Investigation of the working behavior of the proposed kernel estimation function. (a) Visualization of the estimated blur kernel from the Eq. (6), with $k = 0.1\sigma^2$, σ^2, $10\sigma^2$, and $100\sigma^2$, (b) Estimation error of blur kernel, and visual comparison between the estimated kernels under the optimal condition (solid line) and with those having minimum error values (dashed line).

which is followed by absolute and cropping operation, $C : \mathbb{R}^N \rightarrow \mathbb{R}^M$ to Eq. (5). The resultant PSF can be described as follows:

$$h = C\left(\mathcal{W}(y_m, x, k)\right) = F(y_m, x, k) \tag{6}$$

, where $\mathcal{W}$ represents inverse filtering of y_m with w. Although Eq. (6) is a closed-form solution, the uncertainty of mPSD of noise and blur kernel prevents computation. In the case of the Eq. (2), noise-to-signal ratio η should be carefully selected for successful reconstruction [8, 12]. Similarly, optimal blur kernel estimation requires the appropriate noise suppression factor k. The optimal value for k is derived and analyzed in the following.

Claim 2. *Given Gaussian noise $\sim \mathcal{N}(0, \sigma^2)$, the optimal noise suppression factor is given as $k \simeq A(\sigma)^2$, where A represents the smoothness of blur kernel.*

As we have discussed, the noise suppression factor in Eq. (5) is the ratio between mPSD of noise and blur kernel which is analytically derived. According to the *Wiener-Khintchine theorem*, the power spectral density of a random process can be expressed as the Fourier transform of auto-correlation [20, 21]. In the case of Gaussian noise $\sim \mathcal{N}(0, \sigma^2)$, the auto-correlation is defined as $R_{nn}(\tau) = \sigma^2\delta(\tau)$ so its Fourier transform, i.e. mPSD, is : $S_{N_g} = \sigma^2$. Although the mPSD of the blur kernel rarely is known, it represents the smoothness of the blur kernel. Here, we empirically found that $A \simeq 1$ for sparse blur kernel such as motion blur while $A \simeq 100$ for smooth blur kernel such as Gaussian blur.

To see how the noise suppression factor affects the reconstruction quality of the blur kernel, we reformulate the Eq. (5) as follows:

$$\widehat{H} = \frac{\overline{X}}{|X|^2 + k}(HX + N_g) = H + H\left(\frac{-k + \overline{X}N_g/H}{|X|^2 + k}\right) \tag{7}$$

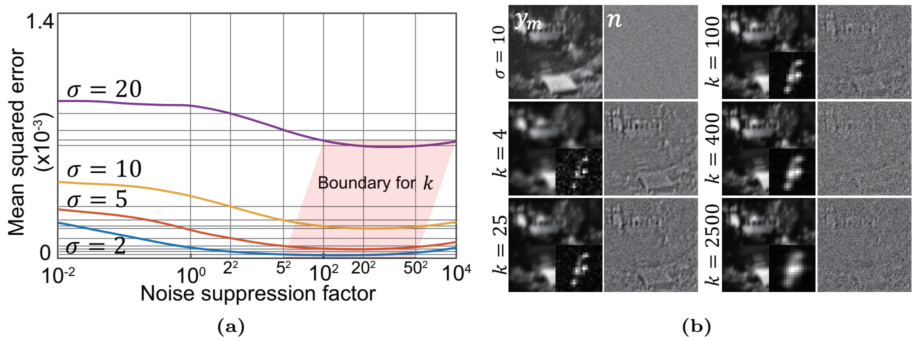

Fig. 2: (a) Illustration of the mean squared error between the measured blurry image y_m and the estimated blurry image y_{est}. (b) Visual comparison of the y_m and $y_m - y_{est}$ for different k. The inset shows the estimated blur kernel.

Fig. 1 (a) shows the reconstructed blur kernel for different noise suppression factors. When $k = \sigma^2$, the proposed kernel estimation function accurately reconstructs the kernel even in strong noise. However, when k is small compared to the noise level, *i.e.* $k \ll \frac{\overline{X}N_g}{H}$, Eq. (7) can be expressed as $\widehat{H} = H + \frac{N_g}{X}$. As shown in Fig. 1 (a) where $k = 0.1\sigma^2$, the Fourier spectrum of noise normalized by the spectrum of a clear image, *i.e.* $\frac{N_g}{X}$, is added to the blur kernel which leads to severe degradation of the reconstructed blur kernel. On the other hand, when k is too large, i.e. $k \gg \frac{\overline{X}N_g}{H}$, Eq. (7) can be expressed as $\widehat{H} = H(1 - \frac{k}{|X|^2+k})$. As shown in Fig. 1 (a) where $k = 10\sigma^2$ and $k = 100\sigma^2$, since the high-frequency spectrum of H becomes zero due to the $\frac{k}{|X|^2+k} \approx 1$, the blur kernel exhibits as a low-pass filtered. Also, Fig. 1 (b) demonstrates that the proposed optimal condition closely approximates the minimization of kernel estimation error. The further analysis for F is described in Supplementary S1.

3.3 Multiple kernel estimation for unknown noise level

A classical strategy to solve inverse problems including blind deblurring is minimizing penalized least square (PLS) methods. The data-fidelity term in PLS formulation of the blind deblurring problem is: $\mathrm{argmin}_{x,h}\|y_m - x * h\|_2^2$. In our cases, as h can be estimated through F, the data-fidelity term can be expressed as $\mathrm{argmin}_x\|y_m - x * F(y_m, x, k)\|_2^2$, which requires setting of k for optimization. However, because we cannot accurately determine the noise level, setting the optimal k is extremely challenging. Nevertheless, since F is a closed-form inverse mapping function, which minimizes Eq. (3), deviating from the optimal condition of k results in increased noise or blurriness rather than leading to incorrect solutions. In other words, even if the k value is not strictly set, as long as it falls within a certain boundary, the data-fidelity term can be minimized. We verified this by examining the mean squared error (MSE) between y_m and

(a) Blur **(b)** GT **(c)** x_0 **(d)** x_1 and h_1 **(e)** x_2 and h_2 **(f)** x_3 and h_3

Fig. 3: Visualization of the blind deblurring results using the multiple kernel estimation scheme. (a) Blurry image degraded with Gaussian noise level of $\sigma = 20$, (b) ground truth, (c) reconstructed clear image, and estimated intermediate image and blur kernels with (d) $k = 5^2$, (e) $k = 15^2$, and (f) $k = 25^2$.

$y_{est} = x * F(y_m, x, k)$ by changing k. As shown in Fig. 2 (a), the MSE decreases as k approaches the optimal condition. Also, the lower error value is maintained over a large range of k, and there exists a range around the optimal suppression factor where $|y_m - x * F(y_m, x, k)| \leq \varepsilon$ even if h is not optimally estimated (Fig. 2 (a) red box). Fig. 2 (b) further demonstrates this by visually comparing y_{est}, $F(y_m, x, k)$, and differential map $y_m - y_{est}$ for different k values when noise level is $\sigma = 10$. Based on this observation, we propose a multiple kernel estimation scheme that handles a wide range of unknown noise levels by setting multiple values for k, rather than a specific value as follows:

$$h_i = F(y_m, x_i, k_i), \qquad \forall i = 1, ..., N_k \tag{8}$$

, where h_i is the estimated blur kernel given intermediate image x_i and k_i is noise suppression factors corresponding to different noise levels. The fundamental concept of this framework lies in managing unknown noise levels by setting k_i from low to high, thus covering a broad range of noise that exists in nature. Here, we also introduce intermediate images, which are separately estimated from a clear image, to compensate for the error term in Eq. (7) caused by a suboptimal setting of k, thereby stabilizing the optimization process. Fig. 3 shows an example of deblurred image x_0, estimated intermediate images x_i and blur kernels h_i. A detailed analysis for intermediate images and the performance of multiple kernel estimation scheme, compared to case where noise level is precisely known, are presented in Supplementary S2. We demonstrate that the proposed multiple kernel estimation scheme exhibits deblurring performance comparable to cases where the noise level is precisely known, and see for the detailed analysis.

3.4 MAP approach for blind deblurring

Conventionally, the MAP approach for blind deblurring is described as follows:

$$p(x, h|y) \propto p(y|x, h)p(x)p(h) \tag{9}$$

, where $p(y|x, h)$, $p(x)$, and $p(h)$ correspond to data-fidelity term, clear image prior, and blur kernel prior, respectively. Many previous works carefully designed the priors to strictly confine the feasible solution space.

In this work, we show that leveraging the capabilities of DIP allows solving

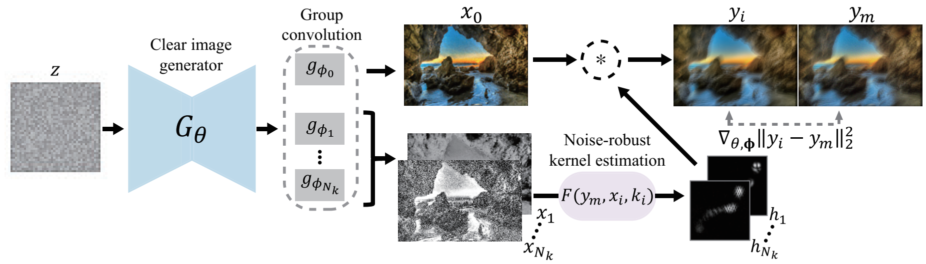

Fig. 4: Workflow of the proposed method. A single deep neural network generates the deblurred image x_0, and the intermediate images x_i which are used to estimate blur kernel h_i with the noise suppression factor k_i.

the blind deblurring problem by estimating solely a clear image even in the presence of noise. Specifically, as blur kernel can be analytically obtained from Eq. (6) if clear image x and blurry image y_m are given, Eq. (9) can be reformulated as follows:

$$p(x, h|y) = p(h|x, y)p(x|y) \propto p(y|x)p(x) \tag{10}$$

As shown in Eq. (10), it is evident that the blind deblurring problem can be addressed by solely focusing on estimating a clear image, while also effectively handling noise owing to the robustness of the proposed kernel estimation function. Therefore, we aim to utilize DIP, one of the optimal methods for estimating natural images.

3.5 Blind deblurring based on noise-robust kernel estimation

We formulate the noise-robust blind deblurring method as follows:

$$\begin{aligned}
&\min_{x_0, h_1, \cdots, h_{N_k}} \frac{1}{N_k} \sum_{i=1}^{N_k} ||y_m - x_0 * h_i||_2^2 + \lambda R(x_0) \\
&s.t.\ x_0 = g_{\phi_0}(G_\theta(z)),\ h_i = F(y_m, g_{\phi_i}(G_\theta(z)), k_i) \\
&h_i^j \geq 0, \sum_j h_i^j = 1 \quad \forall j = 0, 1, \cdots, M
\end{aligned} \tag{11}$$

, where z is fixed tensor randomly sampled from uniform distribution, $(\cdot)^j$ denotes j-th elements, g_{ϕ_i} is i-th group convolution filter convolved with the last feature layer of G_θ to generate x_i, $R(\cdot)$ is regularization function for x_0, and λ is regularization weight. Although we adopt total variation for $R(\cdot)$, other regularization functions such as l_0-sparsity or l_1/l_2 norm can be used.

As shown in Eq. (11), the blind deblurring problem can be solved by focusing on estimating x. Also, it should be noted that the estimation of x_0 and x_i can be achieved with a single neural network as x_i should have a similar appearance with x_0.

Algorithm 1 Blind deblurring with the noise-robust kernel estimation function

Input: Blurred image y_m, pre-defined $\epsilon, \lambda_1, \lambda_2, k_1, k_2, \cdots, k_{N_k}$
Output: clear image x_0 and estimated blur kernels $h_1, h_2, \cdots, h_{N_k}$
Sample z from uniform distribution
for $t = 1$ **to** N_{iter} **do**
  $[f_0, f_1, ..., f_{N_k}] = G_\theta(z)$
  $x_0 = g_{\phi_0}(f_0)$
  $\mathcal{L}_{tot} = 0$
  for $i = 1$ **to** N_k **do**
    $h_i = F(y_m, g_{\phi_i}(f_i), k_i)$
    $h_i = |h_i|$ ▷ Non-negativity
    $h_i = h_i / (\sum h_i + \epsilon)$ ▷ Eqauiltity
    $\mathcal{L}_{tot} = \mathcal{L}_{tot} + \frac{1}{N_k}\left(||y_m - x_0 * h_i||_2^2 + \lambda_1 ||\mathcal{W}(y_m, g_{\phi_i}(f_i), k_i)||_2^2\right)$
  end for
  $\mathcal{L}_{tot} = \mathcal{L}_{tot} + \lambda_2 TV(x_0)$
  Update $\{\theta, \boldsymbol{\phi}\}$ using $\nabla_{\theta,\boldsymbol{\phi}} \mathcal{L}_{tot}$
end for
return $x_0, h_1, h_2, \cdots, h_{N_k}$

3.6 Optimization of the proposed method

The workflow of the proposed method is illustrated in Fig. 4 and the network parameters $\theta, \boldsymbol{\phi} = \{\phi_0, ...\phi_{N_k}\}$ are optimized by the following cost function:

$$\begin{aligned} \min_{\theta, \phi_0, ...\phi_{N_k}} \frac{1}{N_k} \sum_{i=1}^{N_k} (||y_m - g_{\phi_0}(G_\theta(z)) * F(y_m, g_{\phi_i}(G_\theta(z)), k_i)||_2^2 \\ + \lambda_1 ||\mathcal{W}(y_m, g_{\phi_i}(G_\theta(z)), k_i)||_2^2) + \lambda_2 TV(g_{\phi_0}(G_\theta(z))) \\ s.t.\ F(y_m, g_{\phi_i}(G_\theta(z)), k_i)^j \geq 0, \\ \sum_j F(y_m, g_{\phi_i}(G_\theta(z)), k_i)^j = 1 \quad \forall j = 0, 1, \cdots, M \end{aligned} \tag{12}$$

, where TV is total variation, and λ_1 and λ_2 are regularization weights. The non-negativity and equality constraints to the estimated blur kernel are induced by taking an absolute operation followed by dividing each element by the sum of all elements. Also, we additionally introduce a sparsity regularization term for the inverse filtered image, $\mathcal{W}(y_m, g_{\phi_i}(G_\theta(z)), k_i)$, as all pixels except for the blur kernel positioned should have a value of 0. It is important to emphasize that our proposed multiple kernel estimation scheme, rather than regularization terms, is the key enabler for robust deblurring (see the ablation study in Supplementary S7). The optimization of Eq. (12) is formally summarized in Algorithm 1.

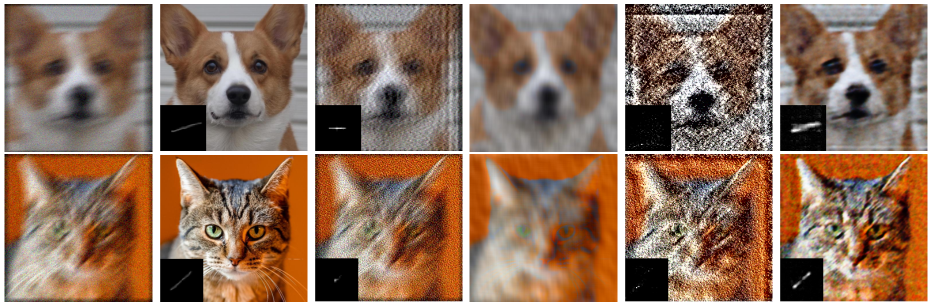

(a) Blur **(b)** GT **(c)** l_1/l_2 **(d)** Pure-let **(e)** WDIP **(f)** Ours

Fig. 5: Qualitative comparison of blind deblurring results on AFHQ datasets [6]. (row 1): AFHQ-dog motion deblurring with a kernel size of 43×43 and noise level of $\sigma = 10$, (row 2): AFHQ-cat motion deblurring with a kernel size of 39×39 and noise level of $\sigma = 20$. Here, the estimated kernel for $k_2 = 15^2$ is presented in (f) while others are presented in Supplementary S5.

4 Experiments

4.1 Experiments on simulated image

Motion deblur on AFHQ dataset [6]. To demonstrate the deblurring performance on motion blur, we conduct experiments on AFHQ-dog 256×256 and AFHQ-cat 256×256 datasets. Specifically, we select 500 test images as an evaluation dataset. To synthesize motion-blurred images, motion-blur kernels of varying sizes, ranging from 21×21 to 51×51, are randomly generated [7], and each kernel is then convolved with a clear image. Finally, Gaussian noise $\sigma = 10$ and $\sigma = 20$ are added to the synthesized blurry images.

The proposed method (refer Supplementary S3 and S6 for implementation detail) is compared with other state-of-the-art blind deblurring methods including Sanghvi *et al.* [35], Xu *et al.* [40], Pure-let [24], Selfdeblur [33], WDIP [3], l_1/l_2 [18], Pan-DCP [30], Pan-l_0 [29], and Liang *et al.* [4], and see Supplementary S4 for implementation details. Note that we exclusively choose blind deblurring methods that do not utilize any training dataset to ensure a fair comparison. When optimizing the proposed method, $k_1 = 5^2$, $k_2 = 15^2$, and $k_3 = 25^2$ are set to accommodate a wide range of unknown noise levels. The representative blind deblurring results from l_1/l_2, Pure-let, WDIP, and the proposed method are qualitatively compared in Fig. 5. Due to the severe degradation caused by Gaussian noise in blurred images, the deblurring results obtained from the compared methods are greatly compromised. Even with laborious adjustment of hyperparameters, these methods tend to overfit strongly to the noise. In contrast, the deblurring results from the proposed method shown in Fig. 5 (f) demonstrate noise-robust deblurring by effectively reconstructing clear images and blur kernels simultaneously even in the absence of precise knowledge about the noise level. Furthermore, quantitative comparison presented in Tab. 1 indicates that the proposed method achieves state-of-the-art performance in terms of Peak

Table 1: Quantitative comparison of blind deblurring results on AFHQ datasets [6] with different noise levels ($\sigma = 10$ and $\sigma = 20$). **Bold**: best.

	AFHQ-dog				**AFHQ-cat**			
	$\sigma = 10$		$\sigma = 20$		$\sigma = 10$		$\sigma = 20$	
Method	PSNR ↑	SSIM ↑	PSNR ↑	SSIM ↑	PSNR ↑	SSIM ↑	PSNR ↑	SSIM ↑
Proposed	**24.23**	**0.632**	**22.90**	**0.539**	**23.33**	**0.590**	**22.11**	**0.497**
SelfDeblur [33]	13.54	0.107	12.02	0.063	12.83	0.080	11.44	0.046
WDIP [3]	14.11	0.115	12.43	0.066	13.43	0.086	11.90	0.049
l_1/l_2 [18]	19.69	0.335	16.03	0.146	19.36	0.308	15.92	0.140
Pan-DCP [30]	10.24	0.060	7.698	0.024	10.17	0.053	7.713	0.022
Pan-l_0 [29]	8.311	0.031	6.836	0.016	8.262	0.029	6.922	0.016
Liang *et al.* [4]	10.68	0.061	7.711	0.023	10.48	0.057	7.694	0.022
Sanghvi *et al.* [35]	16.84	0.520	16.84	0.522	16.26	0.465	16.38	0.471
Xu *et al.* [40]	16.51	0.398	15.01	0.295	15.94	0.357	14.34	0.258
Pure-let [24]	21.02	0.534	19.94	0.477	20.78	0.482	19.79	0.429

Signal-to-noise ratio (PSNR) and Structural Similarity Index Measure (SSIM). See Supplementary S5 for additional qualitative comparisons of deblurring results and quantiative comparisons at low-noise levels ($\sigma = 2$ and $\sigma = 5$).

Sun *et al.* dataset [38]. To further showcase the capability of the proposed method, we utilize the Sun *et al.* dataset, comprising 80 natural images and 8 blur kernels, resulting in the generation of 640 blurry images. The representative blind deblurring results are presented in Fig. 6. The deblurring results obtained from compared methods - l_1/l_2, Pan-DCP, and WDIP - are catastrophically corrupted when noise increases. Conversely, the proposed method shows superior deblurring results regardless of the noise level. Also, as shown in Tab. 2, the proposed method establishes the state-of-the-art deblurring performance.

4.2 Experiments on scanning electron microsope

Scanning electron microscopes (SEM) provide sub-nanometer resolution images by detecting the back-scattered or emitted electrons from the sample. However, the incident electrons, which determine the shape of the PSF of SEM can be easily distorted when the electron passes through several lenses and coils, see Fig. 7 (a). Additionally, random fluctuations of the incident electrons cause Gaussian noise, significantly compromising image quality, see Fig. 8 (a). Correcting such degradation often requires manual adjustment of system parameters, such as working distance or stigmator, by experts. To automate this correction process image quality assessment based method [17,25,26], bayesian optimization based approach [2,34], and feedback-loop based deep learning approach [22,27,36] have been proposed. Nevertheless, previous methods necessitate iterative measurement of SEM images to determine correction parameters, rendering the process

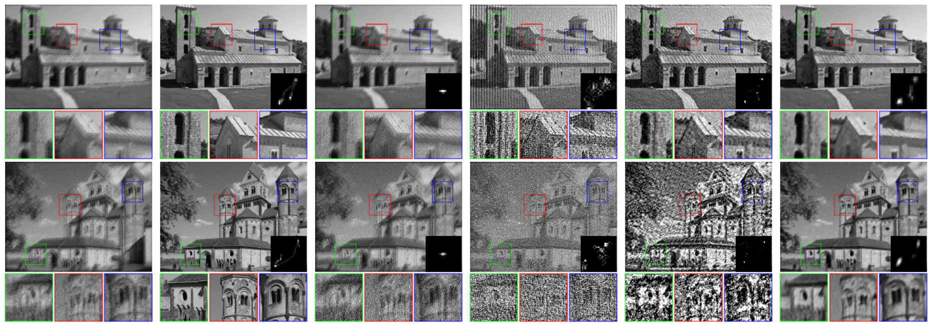

(a) Blur **(b)** GT **(c)** l_1/l_2 **(d)** Pan-DCP **(e)** WDIP **(f)** Ours

Fig. 6: Qualitative comparison of blind deblurring results on Sun *et al.* datasets [38] with Gaussian noise level of (row 1): $\sigma = 10$ and (row 2): $\sigma = 20$. Here, the estimated kernel for $k_2 = 15^2$ is presented in (f) while others are presented in Supplementary S5.

Table 2: Quantitative comparison of blind deblurring results on Sun *et al.* datasets [38] with different noise levels ($\sigma = 10$ and $\sigma = 20$). **Bold**: best.

	$\sigma = 10$		$\sigma = 20$	
Method	PSNR ↑	SSIM ↑	PSNR ↑	SSIM ↑
Proposed	**25.94**	**0.677**	**24.83**	**0.608**
SelfDeblur [33]	17.12	0.202	15.44	0.136
WDIP [3]	17.60	0.214	12.89	0.103
l_1/l_2 [18]	18.87	0.173	14.97	0.073
Pan-DCP [30]	11.62	0.059	8.321	0.021
Pan-l_0 [29]	9.590	0.030	8.065	0.017
Liang *et al.* [4]	11.96	0.060	8.522	0.022
Xu *et al.* [40]	14.10	0.207	13.45	0.128
Pure-let [24]	18.87	0.254	17.31	0.121

time-consuming and energy-inefficient.

Here, we demonstrate the effectiveness of the proposed blind deblurring method in correcting degraded SEM images. In general, well-focused PSF of SEM can be approximated to Gaussian shape [32, 43], we set $A = 100$. Additionally, since the exact noise level of SEM images is rarely known, we set the noise suppression factor in a broad range, such as $k_1 = 10000$, $k_2 = 20000$, and $k_3 = 30000$. Fig. 7 and Fig. 8 presents visual comparisons of blind deblurring results. Although methods such as Pan-DCP or WDIP have successfully performed deblurring on images with weak noise and simple patterns, their performance noticeably deteriorates in cases of strong noise or complex patterns. In contrast, as shown in Fig. 7 (f) and Fig. 8 (f), the proposed method consistently reconstructs both the clear image and the PSF, regardless of the complexity of the image or the level of noise. Especially, as shown in the second row of Fig. 7, when

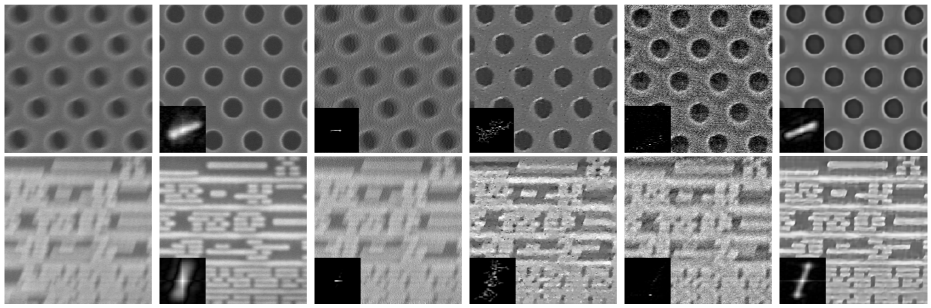

(a) Blur (b) GT (c) l_1/l_2 (d) Pan-DCP (e) WDIP (f) Ours

Fig. 7: Qualitative comparison of blind deblurring results on SEM image of semiconductor. (row 1): Circular ingredient of a semiconductor with the image size of 512×512, (row 2): Wire structure of semiconductor with the image size of 512 × 512. The ground truth PSFs are obtained by the Eq. (6) with $k = 10000$.

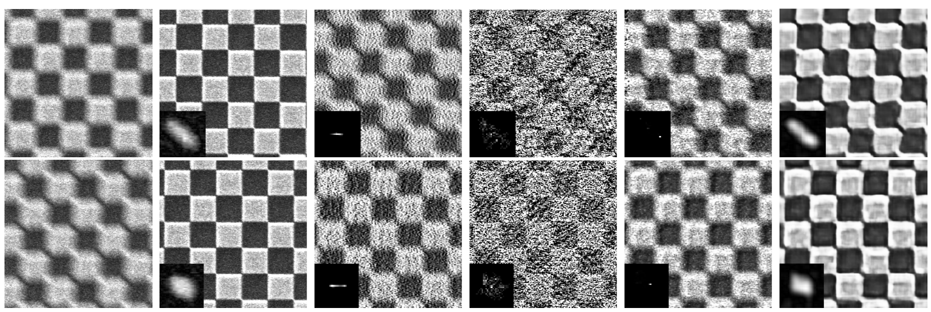

(a) Blur (b) GT (c) l_1/l_2 (d) Pan-DCP (e) WDIP (f) Ours

Fig. 8: Qualitative comparison of blind deblurring results on SEM image severely degraded by noise, with an image size of 256 × 256. The ground truth PSFs are obtained by the Eq. (6) with $k = 10000$.

examining an image with blurred wire patterns, predicting the structure can be challenging even for human observers. However, the deblurred images from the proposed method show a remarkable similarity to the ground truth images and one can effectively investigate the wire structures.

4.3 Experiments on two-photon excitation fluorescence microscope

We further applied the proposed method as one of the real-world applications to a two-photon excitation fluorescence microscope (2PEF) image. In general, the imaging model of 2PEF follows Eq. (1) and its effective PSF can be expressed as the square of illumination PSF [13]. Also, due to the inherent characteristic of weak signals of fluorescence, the measured signal is often contaminated by noise. Here, we captured the fluorescence signal of 2mm beads from the custom-built 2PEF setup. As shown in Fig. 9 (a), the measured image from the 2PEF

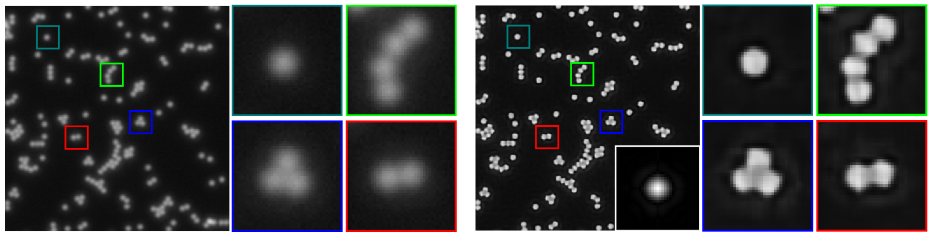

(a) Blur **(b)** Ours

Fig. 9: Visualization of blind deblurring results of the proposed method on blurry two-photon excitation fluorescence microscope image with an image size of 384×384.

exhibits a blurry appearance, attributed to the diffraction limit of the illumination PSF, and is further corrupted by noise. However, when the proposed deblurring method is applied to the measured image, illustrated in Fig. 9 (b), it effectively reconstructs the sharp edges of beads and facilitates easy discernment of clustered beads.

5 Conclusions

In this paper, we propose a noise-robust blind deblurring method combining the multiple kernel estimation scheme and the DIP. The most critical aspect of the proposed method, the noise-robust kernel estimation function, successfully restores the PSF even in situations of high noise when provided only with clear and blurry images. This function is developed to the multiple kernel estimation scheme that can be applied even in scenarios where noise level cannot be accurately predicted. Additionally, by effectively leveraging DIP, which acts as a powerful prior for natural images, we can estimate a clear image from a single well-deigned neural network. The discussion of limitations of the proposed work and ablation study are presented in Supplementary S7. Our proposed method has been demonstrated to operate effectively in both simulated images and real-world applications and outperforms compared to the previous state-of-the-art methods.

Acknowledgements

This work was supported by the Samsung Research Funding and Incubation Center of Samsung Electronics grant SRFC-IT2002-03, Samsung Electronics Co., Ltd. (IO220908-02403-01), and the National Research Foundation of Korea grant funded by the Korean government (Grant Nos. NRF-2021R1A5A1032937, NRF-2021R1C1C1011307, RS-2023-00251628, and RS-2024-00397673).

References

1. Arjomand Bigdeli, S., Zwicker, M., Favaro, P., Jin, M.: Deep mean-shift priors for image restoration. Advances in Neural Information Processing Systems **30** (2017)
2. Binding, J., Mikula, S., Denk, W.: Low-dosage maximum-a-posteriori focusing and stigmation. Microscopy and Microanalysis **19**(1), 38–55 (2013)
3. Bredell, G., Erdil, E., Weber, B., Konukoglu, E.: Wiener guided dip for unsupervised blind image deconvolution. In: Proceedings of the IEEE/CVF Winter Conference on Applications of Computer Vision. pp. 3047–3056 (2023)
4. Chen, L., Fang, F., Lei, S., Li, F., Zhang, G.: Enhanced sparse model for blind deblurring. In: European Conference on Computer Vision. pp. 631–646. Springer (2020)
5. Cho, S., Lee, S.: Fast motion deblurring. In: ACM SIGGRAPH Asia 2009 papers, pp. 1–8 (2009)
6. Choi, Y., Uh, Y., Yoo, J., Ha, J.W.: Stargan v2: Diverse image synthesis for multiple domains. In: Proceedings of the IEEE Conference on Computer Vision and Pattern Recognition (2020)
7. Chung, H., Kim, J., Kim, S., Ye, J.C.: Parallel diffusion models of operator and image for blind inverse problems. In: Proceedings of the IEEE/CVF Conference on Computer Vision and Pattern Recognition. pp. 6059–6069 (2023)
8. Dhawan, A.P., Rangayyan, R.M., Gordon, R.: Image restoration by wiener deconvolution in limited-view computed tomography. Applied optics **24**(23), 4013–4020 (1985)
9. Dong, J., Pan, J., Sun, D., Su, Z., Yang, M.H.: Learning data terms for non-blind deblurring. In: Proceedings of the European Conference on Computer Vision (ECCV). pp. 748–763 (2018)
10. Dong, J., Roth, S., Schiele, B.: Deep wiener deconvolution: Wiener meets deep learning for image deblurring. Advances in Neural Information Processing Systems **33**, 1048–1059 (2020)
11. Gandelsman, Y., Shocher, A., Irani, M.: " double-dip": unsupervised image decomposition via coupled deep-image-priors. In: Proceedings of the IEEE/CVF Conference on Computer Vision and Pattern Recognition. pp. 11026–11035 (2019)
12. Gonzalez, R.C.: Digital image processing. Pearson education india (2009)
13. Helmchen, F., Denk, W.: Deep tissue two-photon microscopy. Nature methods **2**(12), 932–940 (2005)
14. Jin, M., Roth, S., Favaro, P.: Noise-blind image deblurring. In: Proceedings of the IEEE Conference on Computer Vision and Pattern Recognition. pp. 3510–3518 (2017)
15. Jin, M., Roth, S., Favaro, P.: Normalized blind deconvolution. In: Proceedings of the European Conference on Computer Vision (ECCV). pp. 668–684 (2018)
16. Joshi, N., Szeliski, R., Kriegman, D.J.: Psf estimation using sharp edge prediction. In: 2008 IEEE Conference on Computer Vision and Pattern Recognition. pp. 1–8. IEEE (2008)
17. Kawasaki, T., Nakano, T., Hirose, K.: Developing an aberration-corrected schottky emission sem and method for measuring aberration. Microelectronic engineering **86**(4-6), 1017–1020 (2009)
18. Krishnan, D., Tay, T., Fergus, R.: Blind deconvolution using a normalized sparsity measure. In: CVPR 2011. pp. 233–240. IEEE (2011)
19. Kruse, J., Rother, C., Schmidt, U.: Learning to push the limits of efficient fft-based image deconvolution. In: Proceedings of the IEEE International Conference on Computer Vision. pp. 4586–4594 (2017)

20. Kubo, R., Toda, M., Hashitsume, N.: Statistical physics II: nonequilibrium statistical mechanics, vol. 31. Springer Science & Business Media (2012)
21. Lampard, D.: Generalization of the wiener-khintchine theorem to nonstationary processes. Journal of Applied Physics **25**(6), 802–803 (1954)
22. Lee, W., Nam, H.S., Kim, Y.G., Kim, Y.J., Lee, J.H., Yoo, H.: Robust autofocusing for scanning electron microscopy based on a dual deep learning network. Scientific reports **11**(1), 20933 (2021)
23. Levin, A., Weiss, Y., Durand, F., Freeman, W.T.: Understanding and evaluating blind deconvolution algorithms. In: 2009 IEEE conference on computer vision and pattern recognition. pp. 1964–1971. IEEE (2009)
24. Li, J., Luisier, F., Blu, T.: Pure-let image deconvolution. IEEE Transactions on Image Processing **27**(1), 92–105 (2017)
25. Lifshin, E., Kandel, Y.P., Moore, R.L.: Improving scanning electron microscope resolution for near planar samples through the use of image restoration. Microscopy and Microanalysis **20**(1), 78–89 (2014)
26. Lu, Y., Zhang, X., Li, H.: A simplified focusing and astigmatism correction method for a scanning electron microscope. AIP Advances **8**(1) (2018)
27. Na, J., Kim, G., Kang, S.H., Kim, S.J., Lee, S.: Deep learning-based discriminative refocusing of scanning electron microscopy images for materials science. Acta Materialia **214**, 116987 (2021)
28. Nan, Y., Quan, Y., Ji, H.: Variational-em-based deep learning for noise-blind image deblurring. In: Proceedings of the IEEE/CVF conference on computer vision and pattern recognition. pp. 3626–3635 (2020)
29. Pan, J., Hu, Z., Su, Z., Yang, M.H.: Deblurring text images via l0-regularized intensity and gradient prior. In: Proceedings of the IEEE Conference on Computer Vision and Pattern Recognition. pp. 2901–2908 (2014)
30. Pan, J., Sun, D., Pfister, H., Yang, M.H.: Blind image deblurring using dark channel prior. In: Proceedings of the IEEE conference on computer vision and pattern recognition. pp. 1628–1636 (2016)
31. Perrone, D., Favaro, P.: Total variation blind deconvolution: The devil is in the details. In: Proceedings of the IEEE Conference on Computer Vision and Pattern Recognition. pp. 2909–2916 (2014)
32. Reimer, L.: Scanning electron microscopy: physics of image formation and microanalysis. Measurement Science and Technology **11**(12), 1826–1826 (2000)
33. Ren, D., Zhang, K., Wang, Q., Hu, Q., Zuo, W.: Neural blind deconvolution using deep priors. In: Proceedings of the IEEE/CVF Conference on Computer Vision and Pattern Recognition. pp. 3341–3350 (2020)
34. Roels, J., Aelterman, J., De Vylder, J., Luong, H., Saeys, Y., Philips, W.: Bayesian deconvolution of scanning electron microscopy images using point-spread function estimation and non-local regularization. In: 2016 38th Annual International Conference of the IEEE Engineering in Medicine and Biology Society (EMBC). pp. 443–447. Ieee (2016)
35. Sanghvi, Y., Mao, Z., Chan, S.H.: Structured kernel estimation for photon-limited deconvolution. In: Proceedings of the IEEE/CVF Conference on Computer Vision and Pattern Recognition. pp. 9863–9872 (2023)
36. Schubert, P.J., Saxena, R., Kornfeld, J.: Deepfocus: Fast focus and astigmatism correction for electron microscopy. arXiv preprint arXiv:2305.04977 (2023)
37. Shan, Q., Jia, J., Agarwala, A.: High-quality motion deblurring from a single image. Acm transactions on graphics (tog) **27**(3), 1–10 (2008)

38. Sun, L., Cho, S., Wang, J., Hays, J.: Edge-based blur kernel estimation using patch priors. In: IEEE international conference on computational photography (ICCP). pp. 1–8. IEEE (2013)
39. Ulyanov, D., Vedaldi, A., Lempitsky, V.: Deep image prior. In: Proceedings of the IEEE conference on computer vision and pattern recognition. pp. 9446–9454 (2018)
40. Xu, L., Jia, J.: Two-phase kernel estimation for robust motion deblurring. In: Computer Vision–ECCV 2010: 11th European Conference on Computer Vision, Heraklion, Crete, Greece, September 5-11, 2010, Proceedings, Part I 11. pp. 157–170. Springer (2010)
41. Xu, L., Zheng, S., Jia, J.: Unnatural l0 sparse representation for natural image deblurring. In: Proceedings of the IEEE conference on computer vision and pattern recognition. pp. 1107–1114 (2013)
42. Xue, F., Luisier, F., Blu, T.: Multi-wiener sure-let deconvolution. IEEE Transactions on Image Processing **22**(5), 1954–1968 (2013)
43. Zotta, M.D., Nevins, M.C., Hailstone, R.K., Lifshin, E.: The determination and application of the point spread function in the scanning electron microscope. Microscopy and microanalysis **24**(4), 396–405 (2018)
44. Zuo, W., Ren, D., Zhang, D., Gu, S., Zhang, L.: Learning iteration-wise generalized shrinkage–thresholding operators for blind deconvolution. IEEE Transactions on Image Processing **25**(4), 1751–1764 (2016)